Cover Picture: Nanostructural Organization in Acetonitrile/Ionic Liquid Mixtures: Molecular Dynamics Simulations and Optical Kerr Effect Spectroscopy (ChemPhysChem 7/2012)

ARTICLE *in* CHEMPHYSCHEM · MAY 2012

Impact Factor: 3.42 · DOI: 10.1002/cphc.201200026 · Source: PubMed

8 AUTHORS, INCLUDING:

Fehmi Bardak
Celal Bayar Üniversitesi
9 PUBLICATIONS **67** CITATIONS

SEE PROFILE

E. L Quitevis
Texas Tech University
76 PUBLICATIONS **2,025** CITATIONS

SEE PROFILE

DOI: 10.1002/cphc.201200026

VIP

Nanostructural Organization in Acetonitrile/Ionic Liquid Mixtures: Molecular Dynamics Simulations and Optical Kerr Effect Spectroscopy

Fehmi Bardak,[a] Dong Xiao,[b] Larry G. Hines Jr.,[a] Pillhun Son,[a] Richard A. Bartsch,[a] Edward L. Quitevis,*[a] Peng Yang,[c] and Gregory A. Voth*[d]

The nanostructural organization and subpicosecond intermolecular dynamics in mixtures of acetonitrile and the ionic liquid (IL) 1-pentyl-3-methylimidazolium bis{(trifluoromethane)sulfonyl}amide ($[C_5mim][NTf_2]$) are studied as a function of concentration using molecular dynamics (MD) simulations and optical heterodyne-detected Raman-induced Kerr effect spectroscopy. The MD simulations show the IL to be nanostructurally organized into an ionic network and nonpolar domains, with CH_3CN molecules localized in the interfacial region between the ionic network and nonpolar domains, as found previously by other researchers. The MD simulations indicate strong interactions between CH_3CN and the hydrogen atoms on the imidazolium ring of the cation. The low-frequency (0–200 cm^{-1}) intermolecular part of the reduced spectral densities (RSDs) of the mixtures narrows and shifts to lower frequency as the concentration of CH_3CN increases. These spectral changes can be partly attributed to the increasing contribution of the low-frequency intermolecular modes of CH_3CN to the RSD. At a given composition, the RSD of a mixture is found to be broader and higher in frequency than the corresponding ideal RSD given by the volume-fraction-weighted sum of the RSDs of the neat liquids. This difference is rationalized in terms of the competition between CH_3CN–cation interactions and solute-induced disruption of the ionic networks.

1. Introduction

Room-temperature ionic liquids (ILs) are a class of compounds that have been extensively investigated as environmentally benign solvents in synthesis, electrochemistry, separations, and other applications.[1,2] Their potential as green "designer" solvents stems from their negligible vapor pressure, ease of recycling, and the ability to vary their properties by changing the structure of the ions.[3–5] To optimize the use of ILs for various applications, their physicochemical properties must be understood at a molecular level.

Wang and Voth,[6] using a multiscale coarse-graining MD approach, found that ILs based on the l-alkyl-3-methylimidazolium ion ($[C_nmim]^+$) are nanosegregated into polar domains with the cation rings and anions homogeneously distributed and nonpolar domains formed by the aggregation of alkyl groups for C_4 and longer. This result was subsequently more completely analyzed[7] and also confirmed by all-atom MD simulations.[8,9] Using the all-atom MD method, it was further shown[8] that the polar domains are not isolated but are interconnected in such a way as to form a three-dimensional charge-ordered ionic network permeated by nonpolar domains in a manner resembling that of a swollen gel.

Indirect evidence for this structural heterogeneity has been found in Raman (linear and nonlinear) spectroscopic,[10,11] dielectric relaxation, and optical Kerr effect measurements.[12] However, the experimental observation commonly presented as evidence for this structural heterogeneity is the appearance of a first sharp diffraction peak or prepeak at $Q_{MAX} < 0.5$ Å^{-1} in the small-wide angle X-ray scattering (SWAXS) data corresponding to a correlation length $D = 2\pi/Q_{MAX}$ that varies linearly with alkyl chain length. This prepeak has been observed in imidazolium salts with $[BF_4]^-$, $[PF_6]^-$, $[Cl]^-$,[13–15] $[Br]^-$,[16] and bis{(trifluoromethane)sulfonyl}amide ($[NTf_2^-]$),[17–20] in binary mixtures of imidazolium salts,[19,21] in piperidinium-,[22] pyrrolidinium-based salts,[23,24] aliphatic quaternary salts,[25–27] and protic ionic liquids (PILs).[28–30]

To obtain a microscopic understanding of this prepeak, Hardacre et al.[15] performed small-angle neutron scattering (SANS) measurements on H/D isotopically substituted $[C_nmim][PF_6]$ with $n = 4$, 6, and 8. Difference scattering spectra showed that spatial correlations of the imidazolium headgroup, and to a lesser extent, C_n groups, contribute to the prepeak. In addition, the peak position in real space calculated from the in-

[a] F. Bardak, L. G. Hines Jr., Dr. P. Son, Prof. R. A. Bartsch, Prof. E. L. Quitevis
Department of Chemistry and Biochemistry
Texas Tech University, Lubbock TX 79409 (USA)
E-mail: edward.quitevis@ttu.edu

[b] Dr. D. Xiao
Nanjing Institute of Astronomical Optics & Technology
Nanjing 210042 (P.R. China)

[c] P. Yang
Department of Physics, University of Utah
Salt Lake City UT 84112 (USA)

[d] Prof. G. A. Voth
Department of Chemistry, James Franck Institute
Computation Institute, University of Chicago
5735 S. Ellis Avenue, Chicago IL 60637 (USA)
E-mail: gavoth@uchicago.edu

Supporting information for this article is available on the WWW under http://dx.doi.org/10.1002/cphc.201200026.

verse of the peak position in *Q*-space of these ILs and the maximum second-shell cation–cation separation in the radial distribution function (RDF) for $[C_1mim][PF_6]$ derived from SANS data exhibit a linear dependence on the length of the cation. This relationship between the peak position and the length of the cation led Hardacre et al. to propose that the peak is a "result of expansion in the second-shell cation–cation coordination lattice, most probably due to the interspacing of alkyl-chain substituents." They found that spatially resolved probability distributions of anions and cations around a central imidazolium derived from empirical potential structure refinement (EPSR) models are similar for the three ILs with the alkyl chains causing asymmetry in the distributions.

Using an approach that combined computer simulations with X-ray scattering data, Annapureddy et al.[31] sought to clarify further the geometrical origin of the prepeak. The basis for their approach was the observation that for imidazolium-based ILs, the peaks below 2 $Å^{-1}$ in the structure function *S*(*Q*) of the liquid are often found in the powder spectrum of the crystal. By tracking the simulated *S*(*Q*) through the melting transition, Annapureddy et al. showed that these peaks shifted to lower *Q* values with the peak at 0.9 $Å^{-1}$ becoming a shoulder on the peak at 1.5 $Å^{-1}$ in the liquid phase. Simulations of $[C_6mim][Cl]$ and $[C_8mim][PF_6]$ indicate that the way in which polar groups avoid nonpolar groups is the same for the liquid and the crystal. Annapureddy et al. showed, by resolving *S*(*Q*) into subcomponents, that for ILs with short chains the prepeak is attributed to the anion and the nitrogen atoms on the imidazolium ring and not the carbon atoms. This result suggests that the prepeak is associated with an inverse length scale between charged groups. They confirmed that this feature is associated with charged groups separated by the long cationic alkyl tails by comparing the prepeaks in the structure functions of the liquid and the solid. Moreover, Annapureddy et al. found the intensity of the prepeak could be enhanced by artificially bringing the nearest neighbor polar groups closer together.

In a recent study, Castner and co-workers[27,32] combined SWAXS with MD simulations to examine the structure of the IL methyltributylammonium bis{(trifluoromethane)sulfonyl}amide ($[N_{1444}][NTf_2]$) over a wide temperature range, spanning the normal liquid and the glassy state. By resolving *S*(*Q*) into subcomponents, Castner and co-workers also came to the same conclusion as did Hardacre et al. and Annapureddy et al. that the prepeak in the SWAXS data for $[N_{1444}][NTf_2]$ is a consequence of solvation shell asymmetry.

Despite their conclusions, Hardacre et al., Annapureddy et al., and Castner and co-workers neither refuted nor confirmed the existence of complex morphologies. Hardacre et al. stated that "a loosely organized sponge-like microphase defined by ribbons or strings of alternating anions and cations cannot be ruled out." Annapureddy et al. further suggested that the micelle-like and the solvation shell asymmetry interpretations could be just different descriptions of the same liquid morphology in ILs. Santos et al. also posited that their interpretation of the prepeak does not preclude the existence of "highly ordered structures spanning long distances and many ions" in some ionic liquids.

In response to these three studies, Triolo and co-workers[19,21] recently pointed out problems with the assumptions and the supporting evidence underlying this alternate interpretation of the prepeak. Triolo and co-workers, using arguments based on the temperature-dependence of the prepeak, showed that there were issues in the way Hardacre et al. and Annapureddy et al. used X-ray and neutron scattering data for crystalline and liquid-crystalline phases of ILs to support the viewpoint that the prepeak in the isotropic phases of ILs is due to cation asymmetry. Triolo and co-workers also presented new SWAXS data on binary mixtures of ILs with short and long alkyl chains. Instead of two low-*Q* peaks, as would be implied by the cation asymmetry interpretation, they observed a unique prepeak in SWAXS data that varied with composition in a manner consistent with thorough mixing of the alkyl chains. Moreover, they showed that the prepeak disappeared in the SWAXS pattern of $[C_6mim][NTf_2]$ upon replacing the nonpolar C_6 alkyl chain with the polar $CH_3OCH_2CH_2OCH_2$- chain.[19] Similar behavior in the SWAXS data was observed by Hayes et al.[33] and Greaves et al.[30] in going from alkylammonium-based to alkanolammonium-based PILs. That the presence or absence of the low-*Q* peak in the SWAXS data is dependent on the amphiphilicity of the cation for imidazolium-based ILs and PILs can be explained by nanosegregation but not by solvation asymmetry.

MD simulations[8,34,35] indicate that solute–solvent interactions in ILs can be quite complex because of nanosegregation. At low concentrations, solute molecules are found in the domains for which the affinity is the greatest. Nonpolar molecules, such as *n*-hexane, are localized in the nonpolar domains and are excluded from the ionic networks because of the cohesive energy of the charged groups,[8] whereas associating solutes, such as water, are mainly localized in the ionic networks, forming strong hydrogen bonds with the charged parts of the ions.[8,34,35] On the other hand, dipolar molecules, such as CH_3CN, interact with the nonpolar domains as well as with the charged head groups in the ionic networks.[8,34] At high concentrations, the solute molecules eventually disrupt the nanostructural organization and, in the case of water, cause micelles to be formed.[35]

The effect of adding primary *n*-alcohols and hexane to the nanostructural organization in PILs[30] and imidazolium-based ILs[21] has been previously studied using SWAXS. The SWAXS measurements showed the position of the prepeak is unchanged when the alkyl-chain lengths of the *n*-alcohols and the PILs are similar, but changes when the alkyl-chain lengths are different. In contrast, only minor changes in the position of the prepeak are observed with increasing content of hexane. In the case of imidazolium-based ILs, the addition of *n*-alcohols and hexane causes the position of the prepeak to change. This difference between the behavior of PILs and that of imidazolium-based ILs upon addition of solute molecules is attributed to the ionic networks being strongly hydrogen-bonded in PILs as opposed to being weakly hydrogen-bonded in imidazolium-based ILs.

Herein, we report a study of the nanostructural organization and subpicosecond intermolecular dynamics of mixtures of CH_3CN and $[C_5mim][NTf_2]$ using all-atom MD simulations and

optical heterodyne-detected Raman-induced Kerr effect spectroscopy (OHD-RIKES). Although CH_3CN/IL systems have been previously studied by using MD simulations to understand properties such as diffusion constants, viscosities, heats of vaporization and excess properties,[36] and experimentally by using terahertz (THz) spectroscopy[37] and Brillouin light scattering[38] to clarify the nature of the interactions between the components and by time-resolved Stokes shift techniques to understand their solvation dynamics,[39] the current paper, to our knowledge, is the first molecular-level study of CH_3CN/IL mixtures combining MD simulations with OHD-RIKES.

OHD-RIKES, which is a nonlinear optical time-domain technique, probes the collective polarizability anisotropy dynamics in liquids.[40–43] By use of a Fourier-transform-deconvolution procedure,[44,45] OHD-RIKES time-domain data can be converted to a reduced spectral density (RSD) or OKE spectrum, which is directly related to the depolarized Rayleigh/Raman spectrum of the liquid. Because it is easy to use and the resultant data are of high quality, OHD-RIKES is a widely accepted method for studying the low-frequency intermolecular modes of liquids[42,43,46] and, in particular, ionic liquids.[12,17,47–63]

The current paper is part of a series of papers on the nanostructural organization and intermolecular dynamics of molecular-solvent/IL mixtures. We previously presented results from a study of mixtures of CS_2 and $[C_5mim][NTf_2]$ as a function of the mole fraction of CS_2.[64] We found that the CS_2 contribution to the OKE spectrum of a 5 mol% $CS_2/[C_5mim][NTf_2]$ mixture is similar to that of a 5 mol% CS_2/*n*-pentane mixture.[65] This result is consistent with MD simulations that showed the CS_2 molecules to be separated from each other and located in the interior of the nonpolar domains.[64] We also provided further analysis of the OKE spectra of 15–25 mol% mixtures as well as MD simulations of the 20 mol% mixture that showed nanostructural organization at higher solute concentrations to be quite different than at lower concentrations due to aggregation of the CS_2 molecules.

Herein, we discuss how OKE spectra and MD simulations provide support for the localization of CH_3CN molecules in the interfacial region between the ionic network and nonpolar domains and the role of CH_3CN in determining the nanostructural organization and subpicosecond intermolecular dynamics of CH_3CN/IL mixtures. This paper is organized as follows. In Sections 2 and 3, we outline the procedures used to perform the MD simulations and the OHD-RIKES measurements. In Section 4, we present the results of the simulations and Kerr measurements. In Section 5, we discuss the concentration dependence of the RSDs within the context of an additivity model and explain how deviations of the RSDs from this model can be rationalized in terms of effects due to the competition between CH_3CN-cation interactions and solute-induced disruption of the ionic networks.

2. Models and Simulation Methodology

2.1. Atomistic Force Field

The total potential energy is described by the Amber force field given by the expression [Eq. (1)]:

$$V = \sum_{\text{bonds}} k_b(r - r_0)^2 + \sum_{\text{angles}} k_\theta(\theta - \theta_0)^2 + \sum_{\text{dihedrals}} \frac{V_n}{2}(1 + \cos(n\phi - \gamma)) + \sum_i \sum_{j>i} \left(\frac{a_{ij}}{r_{ij}^{12}} - \frac{b_{ij}}{r_{ij}^{6}} + \frac{q_i q_j}{r_{ij}}\right) \quad (1)$$

In the above equation, the force-field parameters for $[C_5mim]^+$ are obtained from the standard Amber force field, while the parameters and partial charges for $[NTf_2]^-$ come from the work of Lopes and Padua,[66] which are compatible with the Amber force field. The partial charges of the cation were calculated by fitting the ab initio electrostatic potentials with the RESP fitting package.[67] The ab initio calculations were performed with Gaussian 03.[68] The force-field and partial charges for CH_3CN used in our simulations were based on the six-site flexible model developed by Nikitin and Lyubartsev.[69]

2.2. Molecular Dynamics Simulation Details

In the simulations, the concentrations of the mixtures investigated were 0, 5, 10, 20, and 50 mol% CH_3CN. The number of ion pairs and CH_3CN molecules depends on the computational feasibility. The simulation parameters are given in Table 1.

Table 1. Sizes for different simulated $CH_3CN/[C_5mim]NTf_2]$ mixtures.

Mole percent CH_3CN	Number of ion pairs	Number of solute molecules	Simulation-cell size (*X*,*Y*, *Z*) [Å]
0	64	0	31.4, 31.4, 31.4
5	76	4	33.4, 33.4, 33.4
10	72	8	32.8, 32.8, 32.8
20	64	16	31.8, 31.8, 31.8
50	64	64	33.1, 33.1, 33.1

The initial configuration of the mixture system was manually constructed, with the ions and CH_3CN molecules positioned within a large cubic simulation box. The initial configuration was simulated at 300 K at constant NPT for 1–2 ns to get a constant volume. The final configuration was then equilibrated at 1000 K under constant NVT conditions and gradually cooled down to 400 K at temperature intervals of 200 K. At each temperature (1000, 800, 600, 400 K), the system was equilibrated for 1.5 ns. The final configuration was then run at 298 K under constant NVT conditions for 8 ns. All simulations were carried out using the DL_POLY 2.19 package[70] with periodic boundary conditions.

2.3. Major Groups and Definitions

The atoms in the system can be divided into three groups: polar, nonpolar, and solute. The polar groups are the positively charged imidazolium ring and the $[NTf_2]^-$ anion, whereas the nonpolar group is the entire alkyl chain. The term "cation headgroup" (or "headgroup") specifically refers to the center of mass of the imidazolum ring. The "tail group" (or "tail") refers to the terminal methyl group on the alkyl chain, which can be approximately described by the carbon atom "CT" in the tail group. The term "NP" refers to the nitrogen atom in the $[NTf_2]^-$ anion, which is used to represent approximately the center of mass of the anion. The terms "H5" and "H4" refer to the hydrogen atoms on the imidazolium ring of the cation. The term "YN'' refers to the nitrogen atom in the CH_3CN molecule. (Definitions of the groups are given in Figure 1).

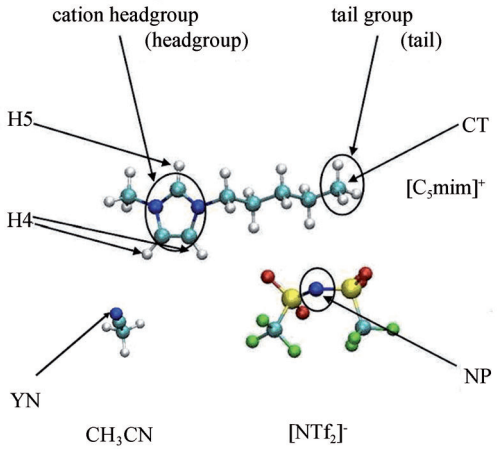

Figure 1. The structures of $[C_5mim]^+$, $[NTf_2]^-$, and CH_3CN. The blue balls represent nitrogen atoms, the cyan balls represent carbon atoms, and the white balls represent hydrogen atoms. The red balls represent oxygen atoms, and the green balls represent fluorine atoms. Atom-type definitions: YN is the nitrogen atom in CH_3CN; NP is the nitrogen atom in the anion; CT is the terminal group on the alkyl chain; and H5, H4 are the hydrogen atoms connected to the cation ring.

3. Experimental Procedure

3.1. Sample Preparation and Characterization

The synthesis of $[C_5mim][NTf_2]$ has been previously described.[71] CH_3CN (Aldrich, spectrochemical grade) was used without further purification. The water content of the freshly synthesized $[C_5mim][NTf_2]$ was determined by Karl Fischer titration to be $<200\ \mu g\,g^{-1}$. The IL was kept in a dessicator to prevent absorption of water. Within the concentration range used in this study, 25–90 mol%, CH_3CN and $[C_5mim][NTf_2]$ were completely miscible and produced mixtures that were optically clear.

Densities of $CH_3CN/[C_5mim][NTf_2]$ mixtures were measured by use of a vibrating tube density meter (Anton Paar DMA 60 and 602) with temperature control from a recirculating bath to an accuracy of $\pm 0.1\%$. In the temperature range of the measurements (283–313 K), densities varied linearly with temperature (see Supporting Information). In Figure 2 are plotted experimental molar volumes of the mixtures at 298.15 K (points) along with the mole fraction

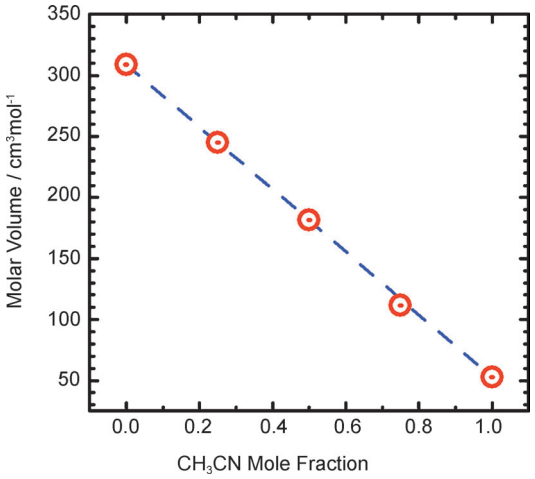

Figure 2. Molar volumes of $CH_3CN/[C_5mim][NTf_2]$ mixtures at 298.15 K. Points are experimental molar volumes and the line is the calculated molar volume using Equation (2).

weighted sum of the molar volumes of the neat liquids [Eq. (2)]:

$$\bar{V}^0_{mix} = X_{ACN}\bar{V}_{ACN} + (1 - X_{ACN})\bar{V}_{IL} \quad (2)$$

where x_{ACN} is the mole fraction of CH_3CN, and $\bar{V}_{ACN}$ and $\bar{V}_{IL}$ are the molar volumes of neat CH_3CN and $[C_5mim][NTf_2]$ (dashed line). As can be seen in this figure, the measured molar volumes are well described by Equation (2). That the molar volumes are additive within experimental error allows us to express the composition of the mixtures by using either the mole fraction or volume fraction of CH_3CN. (Previous studies of the volumetric properties of $CH_3CN/[C_3mim][NTf_2]$ and $CH_3CN/[C_4mim][NTf_2]$ mixtures[72,73] involving density measurements of higher accuracy than in the current study have excess molar volumes of $-1.0\ cm^3\,mol^{-1}$.)

3.2. OHD-RIKES Apparatus and Procedure

The titanium-sapphire (TiS) laser, optical delay line, and pump–probe configuration have been previously reported.[57] Briefly, a Coherent Verdi V6 diode-pumped solid-state laser was used to pump the TiS laser, which generated 36 fs pulses as determined from the pulse-intensity background-free autocorrelation $G_0^{(2)}(t)$. To economize the data collection time, scans were performed in 50 fs steps from -2 to -0.2 ps, in 10 fs steps from -0.2 to 4 ps, and in 50 fs steps from 4 to 10 ps. Pure heterodyne signals were obtained from the difference of data sets obtained at $+5^\circ$ and -5° heterodyne angles, with each data set corresponding to an average of at least 20 scans. Samples for the OHD-RIKES measurements were held in a 2 mm path-length, UV-grade, fused-silica cell (Hellma Cells) with a vacuum stopcock valve. During an OHD-RIKES measurement, the sample was kept at a constant temperature of 295 K using in a laboratory-built copper cell holder and thermoelectric heater/cooler system.

3.3. Analysis of OHD-RIKES Data

The OHD-RIKES responses in the 0.5–10 ps time range are empirically fit by the sum of two exponentials and a constant [Eq. (3)]:

$$R(t) = A_1\exp(-t/\tau_1) + A_2\exp(-t/\tau_2) + B \quad (3)$$

Fits of Equation (3) commonly yield a fast (subpicosecond) component τ_1 and a slow (picosecond) component τ_2 associated with reorientational dynamics.[42] The constant B takes into account contributions to the reorientational dynamics relaxing on a time scale much longer than the time range of our measurements. In this study, a reorientational response was modeled by an empirical impulse function [Eq. (4)]:

$$R(t) = [1-\exp(-2t/\beta)][A_2\exp(-t/\tau_2) + B] \quad (4)$$

In this function, the inertial rise is taken into account by $\beta/2$ where β is equal to $(2\pi c<\omega>)^{-1}$ with $<\omega>$ being the first spectral moment [Eq. (5)]:

$$<\omega> = \frac{\int \omega I(\omega)\mathrm{d}\omega}{\int I(\omega)\mathrm{d}\omega} \quad (5)$$

and $I(\omega)$ being the low-frequency spectral density in the 0–200 cm^{-1} range. The impulse response function in Equation (4) is then convoluted with $G_0^{(2)}(t)$. After "tail-matching," the convoluted reorientational response is subtracted from the OHD-RIKES signal to yield a reduced response, which contains only the electronic and vibrational contributions. The Fourier-transform-deconvolution procedure is applied to the reduced response to obtain the RSD corresponding to the subpicosecond intermolecular dynamics of the liquid. This approach to the analysis of the OKE data in the current study is the same approach used by other research groups in the analysis of the OKE data of IL systems.[48,50–52,55,56,58,59,74] Prior to performing the Fourier-transform-deconvolution procedure, a Gaussian window function is applied to the reduced response.[75] Application of this window function, which eliminates the noise in the RSD, has a negligible effect on the RSDs at high solute concentrations but causes a slight broadening of the RSDs at low solute concentrations.[64]

4. Results

4.1. Nanostructural Organization of CH_3CN/IL Mixtures

In our previous study[64] of CS_2/[C_5mim][NTf_2] mixtures, we showed that because solute–tail interactions are stronger than solute–headgroup or solute–anion interactions, CS_2 molecules are mainly located in the nonpolar domains. In contrast, the probability of finding dipolar solute molecules at or near ionic networks should be higher than in the interior of the nonpolar domains. Figure 3 shows the radial distributions functions (RDFs) between the nitrogen atom in CH_3CN and the center of mass of the imidazolium ring of the cation (YN–headgroup), between the nitrogen atom in CH_3CN and the terminal group of the C_5-chain (YN–CT), and between the nitrogen atom in CH_3CN and the nitrogen atom on $[NTf_2]^-$ (YN-NP) for 5, 10, 20, and 50 mol% CH_3CN/[C_5mim][NTf_2] mixtures. For 5 mol% CH_3CN/[C_5mim][NTf_2], intensities of the first peak in the YN–CT, YN–headgroup, and YN–NP RDFs are 2.09, 2.02, and 1.71, respectively. In contrast, for 5 mol% CS_2/[C_5mim][NTf_2], intensities of the first peak in the CM–CT, CM–headgroup, and CM–NT RDFs are, respectively, 2.25, 1.48, and 1.66, where the term "CM" corresponds to the carbon atom in CS_2. For both CS_2 and CH_3CN at a concentration of 5 mol%, solute-tail interactions are stronger than solute–headgroup and solute–anion interactions. However, based on the relative intensities of the first peak in these RDFs, CH_3CN–headgroup and CH_3CN–anion interactions are stronger than CS_2–headgroup and CS_2–anion interactions, whereas CH_3CN–tail interactions are weaker than CS_2–tail interactions. These results are consistent with previous MD simulations of Lopes and coworkers.[34,76] When the CH_3CN concentration is increased from 5 to 10 mol%, the intensity of the first peak in the YN–CT RDF increases from 2.09 to 2.16, whereas in the YN–headgroup and YN–NP RDFs, it decreases from 2.02 to 1.64 and from 1.71 to 1.52, respectively. We attribute this behavior in the RDFs to a weakening of the interaction of CH_3CN with the ionic networks and the strengthening of its interactions with the nonpolar domains.

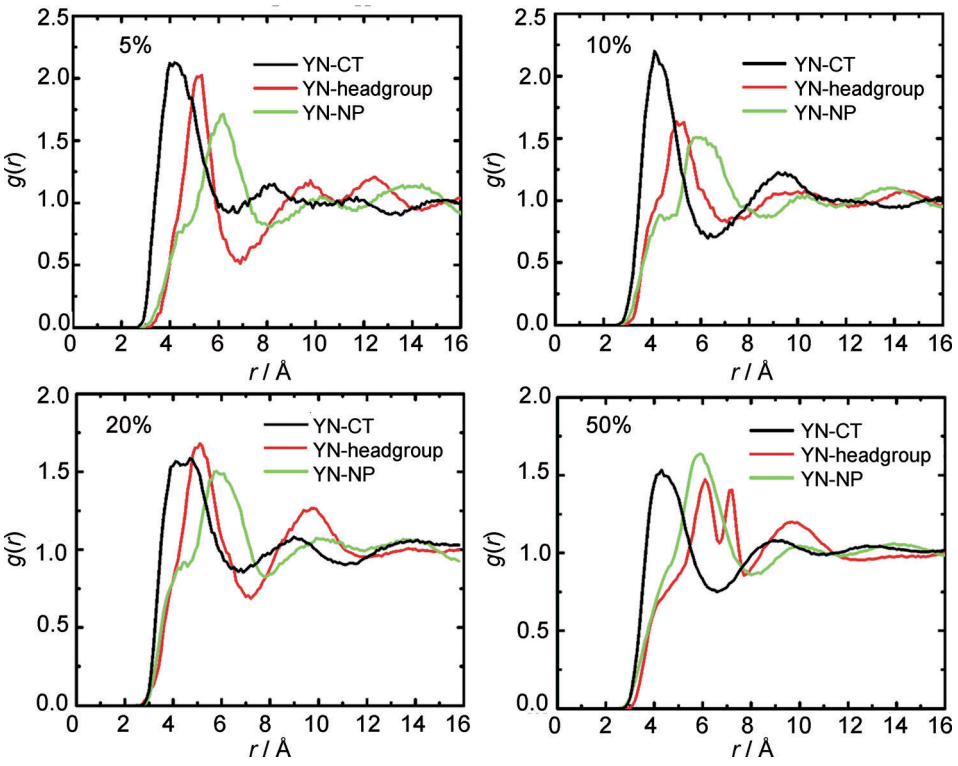

Figure 3. Radial distributions functions for the three important interactions in 5, 10, 20, and 50 mol% CH_3CN/[C_5mim][NTf_2]. YN-headgroup: nitrogen atom in CH_3CN and the cation headgroup; YN-CT: nitrogen atom in CH_3CN and the CH_3 terminal group on the C_5-chain; YN-NP: nitrogen atom in CH_3CN and the nitrogen atom on $[NTf_2]^-$.

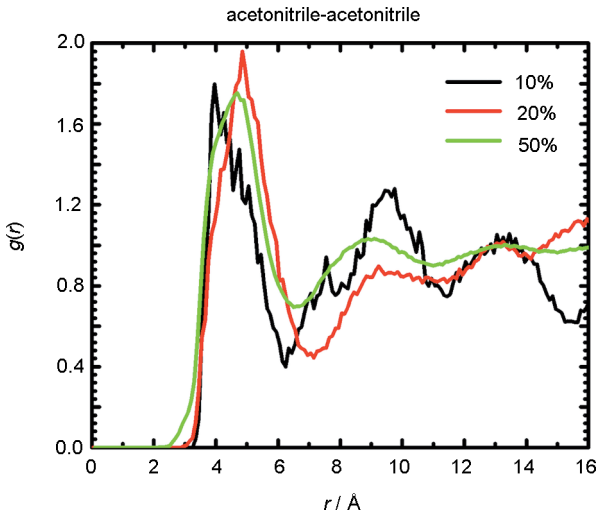

Figure 4. Radial distribution functions between a nitrogen atom on a CH_3CN molecule and a nitrogen atom on a different CH_3CN molecule (acetonitrile–acetonitrile interaction) for 10, 20, and 50 mol% $CH_3CN/[C_5mim][NTf_2]$.

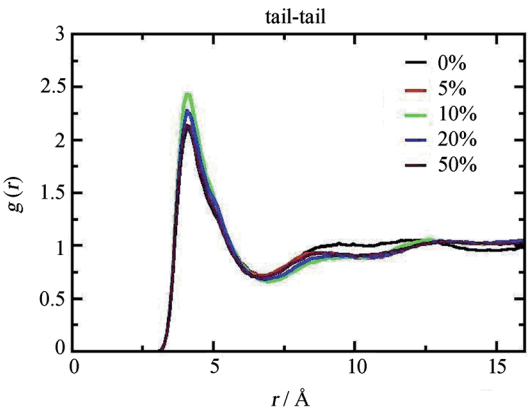

Figure 5. Radial distribution functions between the alkyl tails in $CH_3CN/[C_5mim][NTf_2]$ mixtures.

In the case of 20 and 50 mol% mixtures, the intensities of the first peaks in the three RDFs are very similar. Based on these RDFs, we conclude that the negatively charged nitrogen atom of CH_3CN tends to interact with the positively charged headgroup of the cation and the methyl group on CH_3CN with the nonpolar tail group. These two interactions compete with each other to produce the complicated pattern of peaks in the RDFs at the higher solute concentrations. For example, in the RDF of the 50 mol% mixture, the two close peaks at 6.1 and 7.2 Å in the YN–headgroup RDF suggest that that there two distinct ways in which a CH_3CN molecule can interact with the headgroup of the cation.

Figure 4 depicts the RDF between the nitrogen atom on a CH_3CN molecule and the nitrogen atom on a different CH_3CN molecule (acetonitrile–acetonitrile interaction) for 10, 20 and 50 mol% $CH_3CN/[C_5mim][NTf_2]$ mixtures. That the height of the first peak in this RDF is relatively independent of the CH_3CN mole fraction suggests that aggregation of the CH_3CN is not occurring in these mixture, which is consistent with the observed complete miscibility of CH_3CN with imidazolium-based ILs.[77] In contrast, for $CS_2/[C_5mim][NTf_2]$ mixtures the height of the first peak in CS_2–CS_2 RDF increases with increasing CS_2 mole fraction indicating that aggregation of CS_2 occurs in these mixtures.[64]

In Figure 5 are plotted the RDFs between the alkyl tails in the $CH_3CN/[C_5mim][NTf_2]$ mixtures. These RDFs show no obvious trend with concentration, implying that tail–tail interactions are not directly affected by the presence of CH_3CN in the mixture. In contrast, the MD simulations show strong hydrogen bonding between CH_3CN and the headgroup of the cation, as reflected by the intensity of the first peak in the YN–H4 and YN–H5 RDFs of the $CH_3CN/[C_5mim][NTf_2]$ mixtures as depicted in Figure 6.

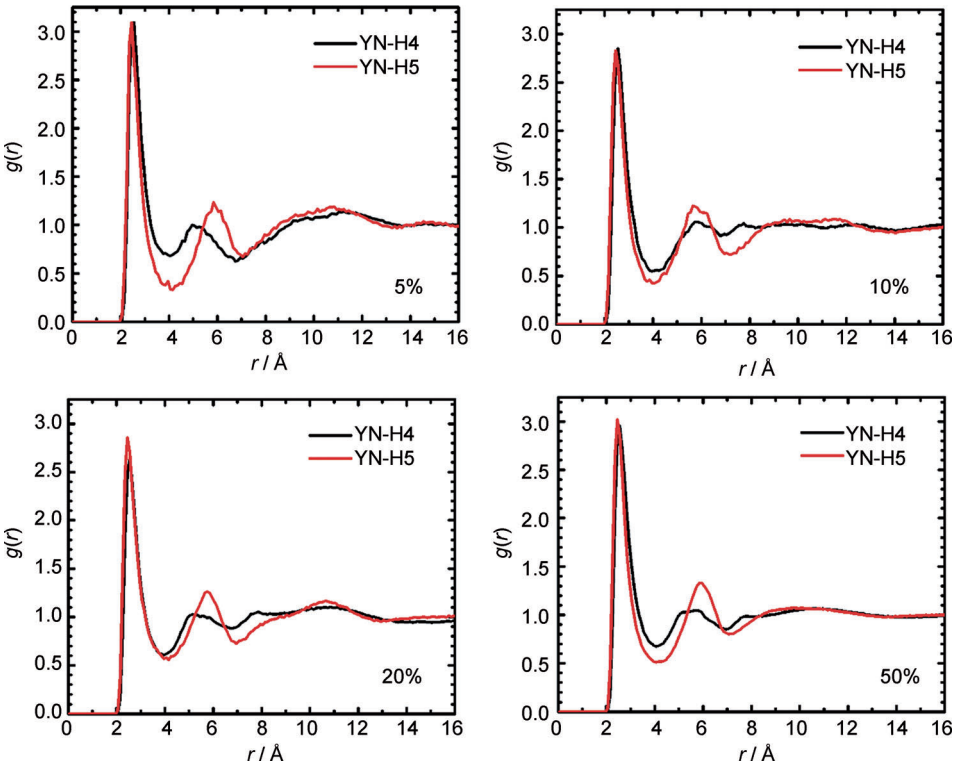

Figure 6. Radial distribution functions between CH_3CN and the hydrogens on the imidazolium ring for 5, 10, 20, and 50 mol% $CH_3CN/[C_5mim][NTf_2]$. YN-H4: nitrogen atom in CH_3CN and the H4 hydrogens on the imidazolium ring. YN-H5: nitrogen atom in CH_3CN and the H5 hydrogen on the imidazolium ring.

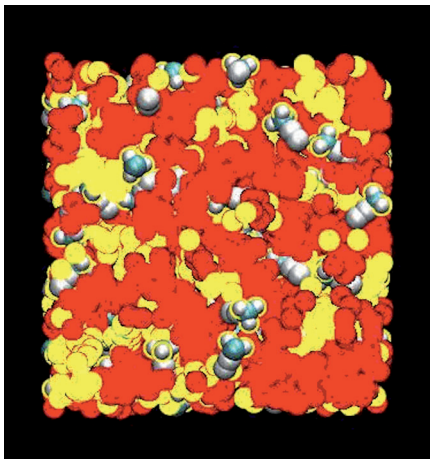

Figure 7. Snapshot of the nanostructural organization in 50 mol% $CH_3CN/[C_5mim][NTf_2]$, with the polar domains color-coded red, the nonpolar domains color-coded yellow, and the CH_3CN molecules represented by space-filling structures.

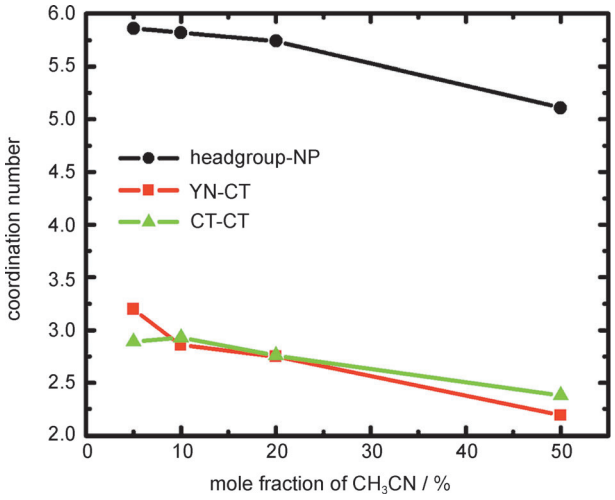

Figure 8. Coordination numbers obtained by integration of the radial distributions: headgroup-NP: cation headgroup and nitrogen atom on $[NTf_2]^-$; YN-CT: nitrogen atom in CH_3CN and the CH_3 terminal group on the C_5-chain; CT-CT: tail-tail.

A representative snapshot of the MD trajectory data obtained during a production run for 50 mol% $CH_3CN/[C_5mim][NTf_2]$ is shown in Figure 7 with the polar domains colored red, the nonpolar domains colored yellow, and the CH_3CN molecules represented by space-filling structures. Snapshots for the other $CH_3CN/[C_5mim][NTf_2]$ mixtures are similar. Snapshots of the MD trajectory data obtained during production runs for 5, 10, and 20 mol% $CS_2/[C_5mim][NTf_2]$ mixtures revealed structures with solute molecules located inside the nonpolar domain (see Figure 3, ref. [54]). However, such structures are not observed for $CH_3CN/[C_5mim][NTf_2]$ mixtures, which we rationalize as being a consequence of the greater affinity of the dipolar solute CH_3CN for the charged groups than for the alkyl chains. Interestingly, in the snapshots, CH_3CN molecules appear to "bridge" the nonpolar and the polar domains, with nitrogen atom of the nitrile group pointing toward the positively charged headgroup of the cation and the methyl group residing in the nonpolar domain, which is similar to what was observed previously by Lopes and co-workers.[8,34]

Figure 8 shows that coordination numbers obtained by integrating the RDFs decrease with increasing concentration of CH_3CN. We attribute the decrease in coordination numbers to the weakening of cation-anion interactions with increasing concentration of CH_3CN. The coordination number of CH_3CN–tail group interaction decreases faster than that of CS_2-tail group interaction. This result reflects the competition between CH_3CN–tail group interactions and CH_3CN-headgroup interactions.

4.2. Intermolecular Dynamics of CH_3CN/IL Mixtures

In principle, the intermolecular and intramolecular modes of both components A and B contribute to the OKE spectra of binary liquid mixtures. If A–B interspecies interactions are different than A–A and B–B interactions, the intermolecular modes in mixtures will be different than those in the neat liquids. This complexity generally makes the interpretation of the OKE spectra of mixtures more difficult compared to the OKE spectra of neat liquids. As recently demonstrated in the case of the OKE spectra of benzene-hexafluorobenzene mixtures,[78] the molecular motions that underlie the OKE spectra can be identified when experiments are performed in concert with MD simulations for mixtures comprised of simple molecules.

The interpretation of the OKE spectra mixtures can be simplified if the Kerr response of one of the components is much larger than that of the other. For example, because the Kerr response of CS_2 is an order of magnitude larger than that of *n*-pentane, the OKE spectrum of a CS_2/*n*-pentane mixture can be treated as arising primarily from the intermolecular vibrational motions of CS_2 molecules in the mixture.[79,80] This simplification also holds for the $CS_2/[C_5mim][NTf_2]$ system at high enough concentrations of CS_2 with the OKE spectrum of the mixture mainly reflecting the intermolecular vibrations of the solute CS_2.[64,65] As will be shown below, the Kerr response of the $CH_3CN/[C_5mim][NTf_2]$ system exhibits behavior different from than that of the $CS_2/[C_5mim][NTf_2]$ system.

4.2.1. OHD-RIKES Signals

In Figures 9 and 10 are plotted the OHD-RIKES signals of $CH_3CN/[C_5mim][NTf_2]$ mixtures normalized at the peak of the coherent spike in the 0–10 ps and 0–2 ps time ranges, respectively, with the signals in Figure 9 offset for clarity. In contrast to CS_2, the intensity of the raw signal at the coherent spike for CH_3CN is roughly a factor of two less than that of $[C_5mim][NTf_2]$. These plots illustrate similarities as well as differences between the Kerr response of an IL and that of a simple molecular liquid such as CH_3CN. The nuclear part of the Kerr response of CH_3CN can be divided into a subpicosecond part associated with the intermolecular dynamics that makes up ~70% of the peak amplitude and a reorientational part with an exponential relaxation time of 1.65 ± 0.05 ps, in agreement with previous measurements.[79–81] The nuclear part of the Kerr

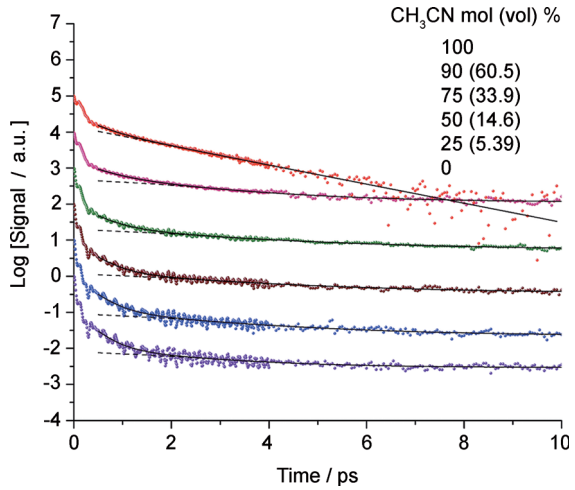

Figure 9. OHD-RIKES signals normalized at the coherent spike ($t=0$) in the 0–10 ps time range for mixtures of CH_3CN in [C_5mim][NTf_2] for different CH_3CN mole fractions. The signals have been offset for clarity. Solid lines are fits of an empirical decay function [Eq. (3)] to the data. Dashed lines are the slow (ps and longer) contributions to the empirical decay function. See Table 2 for fit parameters.

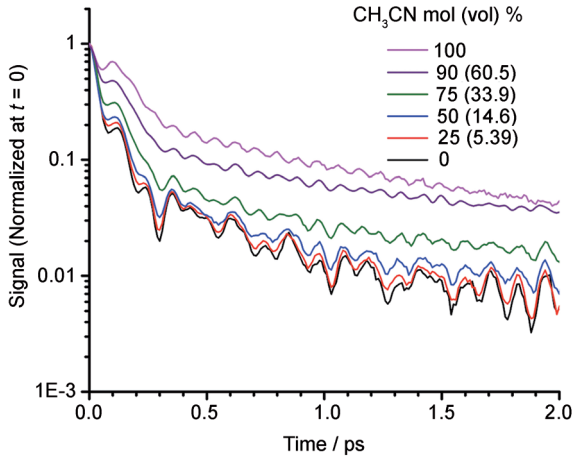

Figure 10. OHD-RIKES signals normalized at the coherent spike ($t=0$) in the 0–2 ps time range for mixtures of CH_3CN in [C_5mim][NTf_2] for different CH_3CN mole fractions.

response of [C_5mim][NTf_2] can similarly be divided into a subpicosecond part associated with the intermolecular dynamics but with a reorientational part that relaxes on a much slower time scale in the time range of our measurements. As recent OKE experiments over a broad range of times (1 ps to hundreds of ns) and temperatures down to the glass transition have shown,[12,82,83] ILs are complex fluids with low-frequency modes characterized by α- and β-relaxations. Due to the limited time range of our OKE apparatus, we are only able to probe molecular motions in ILs associated with the slow and fast β-relaxations, librational motions, and intramolecular vibrations.

The solid lines in Figure 9 are fits of Equation (3) to the experimental decays with fit parameters given in Table 2. The dashed lines in this Figure are the slow (ps and longer) contributions to the empirical decay function represented by the τ_2 component and the constant B in Equation (3). The reorientational dynamics of complex fluids is commonly described at short times (few ps to hundreds of ps) by an intermediate power law and at longer times by a von Schweidler power law and a temperature-dependent exponential (α-relaxation).[83,84] Clearly, an empirical function such as Equation (3) captures only the intermolecular dynamics and a part of the intermediate power law region of the reorientational dynamics. Although a power law could be used to fit the data, the form of the function used to model the reorientational relaxation in the time range of our measurements is not important for the purposes of the current study.

The evolution of the Kerr response in going from neat IL to neat CH_3CN, as illustrated in Figure 10, is very similar to that observed for CS_2/IL mixtures in that increasing the mole fraction of the molecular liquid causes an increase in the amplitude of nuclear part relative to that of the electronic part. Because the Kerr response of CH_3CN is an order of magnitude weaker than that of CS_2, to achieve the same relative change, the concentration of the molecular solute must be increased by a much higher value for CH_3CN than for CS_2. For 25 mol% CH_3CN/IL, the Kerr response hardly differs from that of the neat IL. In contrast, for 25 mol% CS_2/IL, the Kerr response is more like that of CS_2 than that of the IL (see Figure 7 in ref. [54]). Eventually, the Kerr response of the CH_3CN/IL system begins to look more like that of CH_3CN at 90 mol%.

Another feature common to both CH_3CN and [C_5mim][NTf_2] is the underdamped oscillation superimposed on the Kerr responses (Figure 10). In CH_3CN, the oscillation is simple and arises primarily from a single coherently excited low-frequency intramolecular vibration of the molecule, whereas in [C_5mim][NTf_2], the oscillation is complex and arises from the superposition of several coherently excited low-frequency intramolecular vibrations of both the cation and the anion. For the mixtures, the intramolecular vibrations of both liquids contribute to the complex oscillatory structure of the Kerr response. At 25 and 50 mol%, the oscillations in the Kerr responses of the mixtures closely resemble the oscillations in the Kerr response of the neat IL. With increasing mole fraction of CH_3CN, contributions

Table 2. Decay parameters for OHD-RIKES signals for CH_3CN/[C_5mim][NTf_2] mixtures.[a,b]

Mole percent CH_3CN	A_1	τ_1 [ps]	A_2	τ_2 [ps]	B	r[c]
0	0.094 ± 0.012	0.32 ± 0.03	0.009 ± 0.002	2.02 ± 0.48	0.0029 ± 0.0003	0.896
25	0.088 ± 0.009	0.35 ± 0.03	0.010 ± 0.001	2.59 ± 0.56	0.0022 ± 0.0004	0.920
50	0.082 ± 0.007	0.38 ± 0.03	0.010 ± 0.001	2.98 ± 0.56	0.0034 ± 0.0004	0.944
75	0.081 ± 0.004	0.44 ± 0.03	0.019 ± 0.001	3.03 ± 0.37	0.0053 ± 0.0004	0.976
90	0.112 ± 0.004	0.41 ± 0.03	0.064 ± 0.003	2.01 ± 0.11	0.0116 ± 0.0004	0.985
100	0.184 ± 0.005	0.38 ± 0.03	0.277 ± 0.011	1.64 ± 0.03	0	0.994

[a] See Equation (3) for definition of fit parameters. [b] Fit range 0.5–10 ps. [c] Correlation coefficient.

from underdamped oscillations associated with the intramolecular vibrations of CH_3CN begin to appear with the oscillations clearly exhibiting features characteristic of both CH_3CN and the IL for the 75 mol% mixture and largely that of CH_3CN for the 90 mol% mixture.

4.2.2. OKE Spectra

In Figures 11 and 12 are plotted RSDs in the 0–400 cm^{-1} range and 0–200 cm^{-1} range, respectively, obtained by performing the Fourier-transform-deconvolution procedure on the reduced

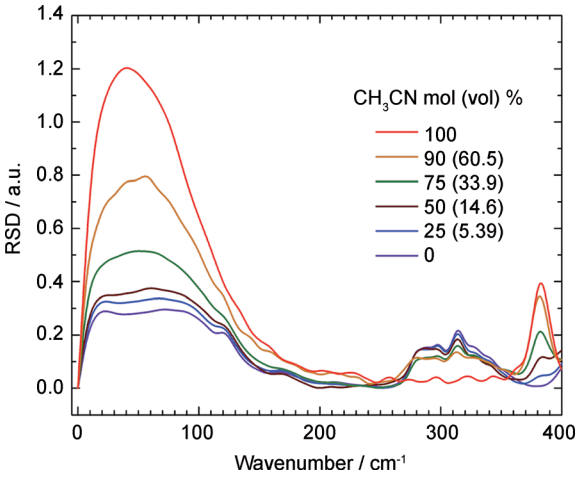

Figure 11. Reduced spectral densities of $CH_3CN/[C_5mim][NTf_2]$ mixtures in the 0–400 cm^{-1} region corresponding to OHD-RIKES signals normalized at $t=0$.

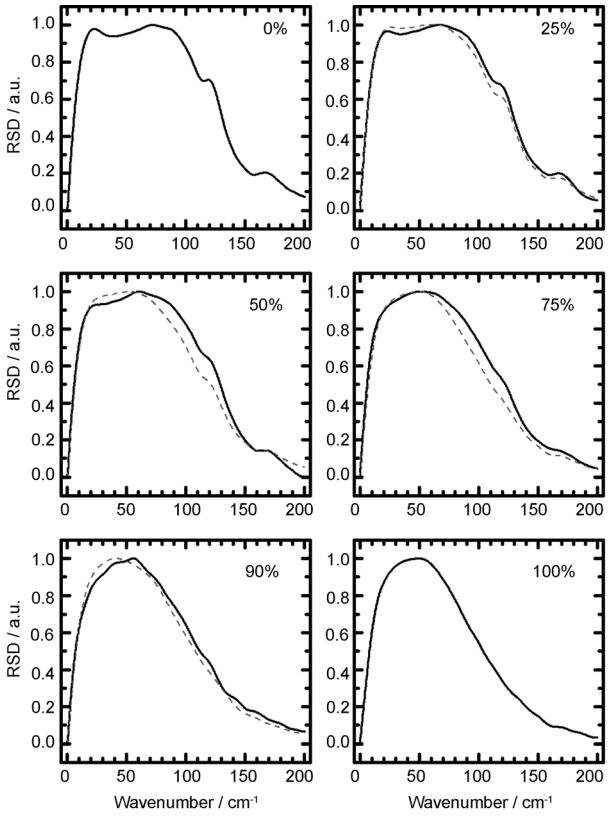

Figure 12. Height-normalized reduced spectral densities of $CH_3CN/[C_5mim][NTf_2]$ mixtures in the 0–200 cm^{-1} region. Solid curves (——): experimentally measured reduced spectral density. Dashed curves (-----): ideal reduced spectral density by taking the volume-fraction-weighted sum of the reduced spectral densities of the neat liquids [Eq. (6)]. See Table 3 for spectral parameters.

Kerr responses. In Figure 11, the RSDs correspond to the OHD-RIKES signals normalized at $t=0$. In Figure 12, the RSDs have been height-normalized. For purposes of discussion, the RSDs in Figure 11 can be divided into two regions: 0–200 cm^{-1} (region A) and 200–400 cm^{-1} (region B). In region B, the series of lines between 260 and 360 cm^{-1} primarily correspond to intramolecular vibrations of $[NTf_2]^-$ and the line at $\approx$382 cm^{-1} to an intramolecular vibration of CH_3CN.

In region A, the RSD of $[C_5mim][NTf_2]$ is characterized by a bimodal intermolecular band with a narrow peak at $\approx$23 cm^{-1} and a broad peak $\approx$68 cm^{-1}. Superimposed on the intermolecular band of $[C_5mim][NTf_2]$ are peaks at 122 and 172 cm^{-1} associated primarily with the intramolecular vibrational modes of the anion and the cation, respectively. Because of the large difference between the third-order polarizability derivative of the imidazolium rings and that of the alkyl chains, the intermolecular part of the RSDs of imidazolium-based ILs mainly reflects the intermolecular dynamics in the ionic networks.[48,53,54] This assignment of the RSD is consistent with a recent study[85] that showed very little dependence of the RSD on the alkyl-chain length for $[C_nmim][NTf_2]$ with $n=3$–10. In contrast, the RSD of CH_3CN is characterized by a single intermolecular band. As can be seen in Figure 12 and Table 3, the RSD of $[C_5mim][NTf_2]$ is higher in frequency and broader ($<\omega>\approx$75 cm^{-1}; $\Delta\omega\approx$125 cm^{-1}) than that of CH_3CN ($<\omega>\approx$67 cm^{-1}; $\Delta\omega\approx$96 cm^{-1}). This difference between the RSD of $[C_5mim][NTf_2]$ and the RSD of CH_3CN is a consequence of the intermolecular dynamics being governed by coulombic and van der Waals interactions in $[C_5mim][NTf_2]$ but only by dipole–dipole interactions in CH_3CN.

In region A, the RSD of the 25 mol% mixture resembles that of neat $[C_5mim][NTf_2]$ with its characteristic intermolecular

Table 3. Spectral parameters for reduced spectral densities of $CH_3CN/[C_5mim][NTf_2]$ mixtures in the 0–200 cm^{-1} region at 295 K.[a,b]

Mole %[c]	Volume %[c]	$<\omega>_{ideal}$[d] [cm^{-1}]	$\Delta\omega_{ideal}$[d] [cm^{-1}]	$<\omega>_{exp}$[e] [cm^{-1}]	$\Delta\omega_{exp}$[e] [cm^{-1}]
0	0	75	125	75	125
25	5.39	73	122	75	124
50	14.6	71	114	72	123
75	33.9	69	103	71	115
90	60.6	68	101	71	105
100	100	67	96	67	96

[a] $<\omega>$: first spectral moment [Eq. (5)]; $\Delta\omega$: full-width-at-half-maximum. [b] Error in $<\omega>$ and $\Delta\omega=\pm1$ cm^{-1}. [c] Mole and volume percent CH_3CN. [d] Spectral parameters for ideal RSD given by the volume-fraction-weighted sum of RSDs of the neat liquids [Eq. (6)]. [e] Spectral parameters for experimental RSDs.

peaks at 23 and 68 cm^{-1} and intramolecular peaks at 122 and 172 cm^{-1} clearly discernible. Upon further dilution, these features disappear with the RSD of the 90 mol% mixture resembling neat CH_3CN more than the IL. This behavior is not surprising as one expects the intermolecular dynamics of the IL-rich mixture to be dominated by the IL and that of the CH_3CN-rich mixture by CH_3CN. More significantly, the RSDs exhibit a narrowing and shift to lower frequency with increasing content of CH_3CN (Table 3). This behavior is similar to what is observed in CS_2/alkane mixtures with increasing content of the alkane solvent. The underlying mechanisms for spectral evolution are however different for the two mixture systems. Because of the large difference between the Kerr response of CS_2 and that of an alkane solvent, the RSD of CS_2/alkane mixtures is mainly attributed to the intermolecular dynamics of CS_2. In CS_2/alkane mixtures, the narrowing and shift to lower frequency of the RSD is attributed to softening of the intermolecular potential upon dilution with a weakly interacting alkane solvent. In contrast, the Kerr response of CH_3CN and the IL are of comparable magnitude. As can be seen in Figure 12, RSDs of CH_3CN/IL mixtures contain contributions from both CH_3CN and the IL. Part of the narrowing and shift to lower frequency with increasing dilution in CH_3CN/IL mixtures simply reflects the increasing contribution of the narrower and lower frequency CH_3CN component to the RSDs of the mixtures. That this mechanism accounts for a large part of concentration dependence of the RSDs is evident when one examines appropriately weighted sums of the RSDs of neat CH_3CN and the neat IL.

5. Discussion

We showed previously that the RSDs of certain binary imidazolium-based IL mixtures comprised of a common cation are well-described by the mole-fraction-weighted sum of the normalized RSDs of the neat ILs.[53,57] The use of mole-fraction weighting in these mixtures is justified by the RSDs of the neat ILs being largely determined by the imidazolium ring as explained above.

Interestingly, the area of the RSD in the 0–200 cm^{-1} region associated with OHD-RIKES signals normalized at $t=0$ varies linearly with the volume fraction of CH_3CN (Figure 13),[86] which suggests that we compare the RSDs of the mixtures in Figure 12 to an additivity model or "ideal" RSD given by the volume-fraction-weighted sum [Eq. (6)]:

$$I_{mix}^{ideal}(\omega) = N\left[f_{ACN}^{vol} I_{ACN}^{neat}(\omega) + \left(1 - f_{ACN}^{vol}\right) I_{IL}^{neat}(\omega)\right] \quad (6)$$

where f_{ACN}^{vol} is the volume fraction of CH_3CN, $I_{ACN}^{neat}(\omega)$ and $I_{ACN}^{neat}(\omega)$ are the RSDs of neat CH_3CN and $[C_5mim][NTf_2]$ in Figure 11, and N is a normalization constant. The use of volume fraction as a measure of composition is not uncommon in OHD-RIKES studies of binary liquid mixtures.[79,80,87,88] Height-normalized RSDs for 25, 50, 75, and 90 mol% CH_3CN/$[C_5mim][NTf_2]$ mixtures calculated by using Equation (6) are shown in Figure 12, with the spectral parameters given in Table 3.

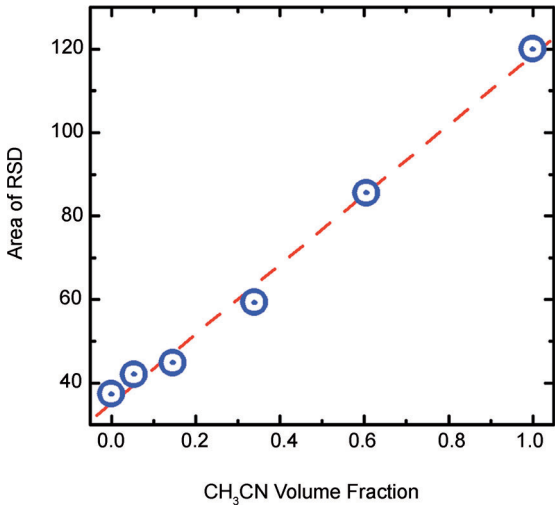

Figure 13. Areas of reduced spectral densities of CH_3CN/$[C_5mim][NTf_2]$ mixtures in the 0–200 cm^{-1} region (Figure 10) as a function of CH_3CN volume fraction, f_{ACN}^{vol}, fit to the linear equation. Area = 83.42 f_{ACN}^{vol} + 35.06, correlation coefficient = 0.99657.

As can be seen in Figure 12, the additivity model with volume-fraction weighting yields quite reasonable agreement with the experimentally observed RSD [$\equiv I_{mix}^{exp}(\omega)$]. Moreover, the dependence of the values of $\Delta\omega_{ideal}$ and $<\omega>_{ideal}$ on composition parallels that of $\Delta\omega_{exp}$ and $<\omega>_{exp}$ (see Table 3), thus lending support to the narrowing and shift to lower frequency being mainly due the increasing contribution of CH_3CN to the RSD. Interestingly, the $I_{mix}^{exp}(\omega)$ are slightly higher in frequency and narrower than $I_{mix}^{ideal}(\omega)$, with the difference being quite noticeable for the 50 and 75 mol% mixtures on the high-frequency side of the RSDs.

Deviations from additivity in binary mixtures are not unexpected when A–B interspecies interactions are comparable in strength to A–A or B–B interactions. The MD simulations suggest that the deviations of the RSDs from additivity are primarily a consequence of changes in the intermolecular dynamics when CH_3CN molecules are dissolved in the IL. It is clear from the snapshots of the nanostructural organization of 10, 20, 50 mol% mixtures (i.e., Figure 7) that CH_3CN molecules are isolated from each other and are in local environments quite different from that in the neat liquid. It is physically reasonable that the intermolecular vibrations of CH_3CN will be different in the mixture than in the neat liquid. The snapshots show the nitrile group in CH_3CN oriented toward the polar domains (see Figure 7), which implies that CH_3CN–IL interactions will be dominated by ion–dipole forces. A CH_3CN molecule as a result sees a stiffer intermolecular potential in CH_3CN/IL mixtures than in the neat liquid where the intermolecular potential is mainly governed by weaker dipole-dipole forces. Within the framework of the additivity model [Eq. (6)], the CH_3CN contribution to the RSD will be different than the RSD of neat CH_3CN because the intermolecular vibrations of CH_3CN will be higher in frequency in the mixtures than in the neat liquid. This is clear when the RSDs of the 25 and 50 mol% mixtures are fit by an empirical line shape function of the form [Eq. (7)]:

$$I_{mix}^{exp}(\omega) = N\left[f_{ACN}^{vol} I_{ACN}^{mix}(\omega) + \left(1 - f_{ACN}^{vol}\right) I_{IL}^{neat}(\omega)\right] \quad (7)$$

This equation is basically the additivity model [Eq. (6)] with the CH_3CN contribution replaced by the quantity $I_{ACN}^{mix}(\omega)$, which we will represent by a three-component line-shape model with the low-frequency component 1 given by a Bucaro–Litovitz function [Eq. (8)]:

$$I_{BL}(\omega) = A_{BL}\omega^{a}\exp(-\omega/\omega_{BL}) \quad (8)$$

and the intermediate- and high-frequency components 2 and 3 by the antisymmetrized Gaussian (AG) line-shape function [Eq. (9)]:

$$I_{AG}(\omega) = A_{AG}\{\exp[-(\omega-\omega_{AG})^2/2\varepsilon^2] - \exp[-(\omega+\omega_{AG})^2/2\varepsilon^2]\} \quad (9)$$

As can be seen in Figure 14, Equation (7) gives reasonable fits of the RSDs for the 25 and 50 mol% mixtures (see Table 4 for the BL and AG fit parameters).

Figure 15 compares the height-normalized $I_{ACN}^{mix}(\omega)$ for the 25 and 50 mol% mixtures to the fit of $I_{ACN}^{neat}(\omega)$ to the three-component line-shape model, with the underlying component bands also shown. If $I_{ACN}^{mix}(\omega)$ is assumed to be the intermolecular spectrum of CH_3CN in mixtures, then the analysis indicates that this spectrum is not only higher in frequency but also broader than that of CH_3CN in the neat liquid ($\omega_{pk}^{mix} = 55\ cm^{-1}$, $\Delta\omega^{mix} = 111\ cm^{-1}$ for 25 mol% and $\omega_{pk}^{mix} = 56\ cm^{-1}$, $\Delta\omega^{mix} = 114\ cm^{-1}$ for 50 mol% versus $\omega_{pk}^{neat} = 41\ cm^{-1}$, $\Delta\omega^{neat} = 95\ cm^{-1}$ for neat CH_3CN). Another interesting feature of the intermolecular spectra of CH_3CN in these mixtures is that they are more structured than that of neat CH_3CN with enhanced shoulders on the low and high frequency sides of the spectra. Whereas the amplitude of the low-frequency component 1 relative to that of the intermediate-frequency component 2 roughly remains constant, the high-frequency component 3 increases in amplitude in going from the 25 mol% mixture to the 50 mol% mixture. The structured nature of these spectra is consistent with the existence of different CH_3CN–cation complexes as indicated by the split first peak in the YN–headgroup RDF for the 50 mol% mixture (Figure 3).

The validity of this analysis clearly hinges on the approximation that the IL contribution to the RSD is given by RSD of the neat IL. Although MD simulations show a decrease in the coordination number in the ionic network (Figure 8), the snapshot of the nanostructural organization for the 50 mol% mixture (Figure 7) shows the ionic networks to be largely unaffected by the presence of CH_3CN, lending credence to this approximation. However, with increasing solute concentration, the presence of CH_3CN molecules eventually leads to the disruption of the ionic networks, softening of the potential governing the intermolecular modes of the IL, and breakdown of the approximation. Solute-induced disruption of the ionic networks has the opposite effect of shifting the RSD of the mixtures to lower frequency. That $I_{mix}^{exp}(\omega)$ for the 75 mol% mixture is still higher in frequency and narrower than $I_{mix}^{ideal}(\omega)$ suggests that solute-induced disruption of the ionic networks plays less of a role in determining the RSD than

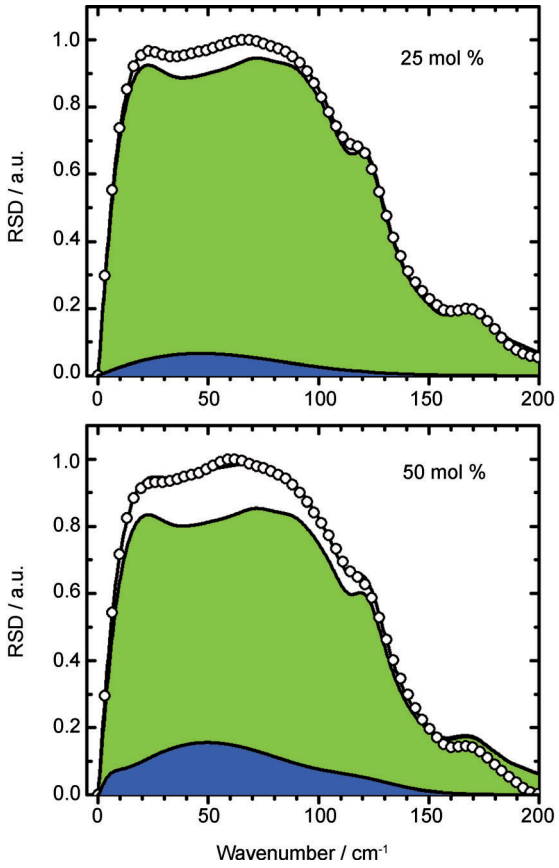

Figure 14. Fits of the empirical line-shape function (line) given by Equation (7) with the IL contribution given by the RSD of neat $[C_5mim][NTf_2]$ (green) and the CH_3CN contribution given by the three-component model (blue) for the RSDs of the 25 and 50 mol% $CH_3CN/[C_5mim][NTf_2]$ mixtures (points).

Table 4. Fit parameters for the three-component line-shape model of the intermolecular spectrum of CH_3CN in $CH_3CN/[C_5mim][NTf_2]$ mixtures.

Mole percent CH_3CN	Bucaro Litovitz[a] (component 1)			Antisymmetrized Gaussian[b] (components 2 and 3)		
	A_{BL}	a	ω_{BL} [cm^{-1}]	A_{AG}	ω_{AG} [cm^{-1}]	ε [cm^{-1}]
25	0.038	1.59	7.3	0.89	49.9	43.3
				0.10	133.9	50.0
50	0.045	1.52	7.2	0.98	56.0	37.5
				0.27	120.0	20.6
100	0.037	1.31	13.0	1.06	47.9	45.3
				0.18	130.9	29.7

[a] See Equation (8) for definition of parameters. [b] See Equation (9) for definition of parameters.

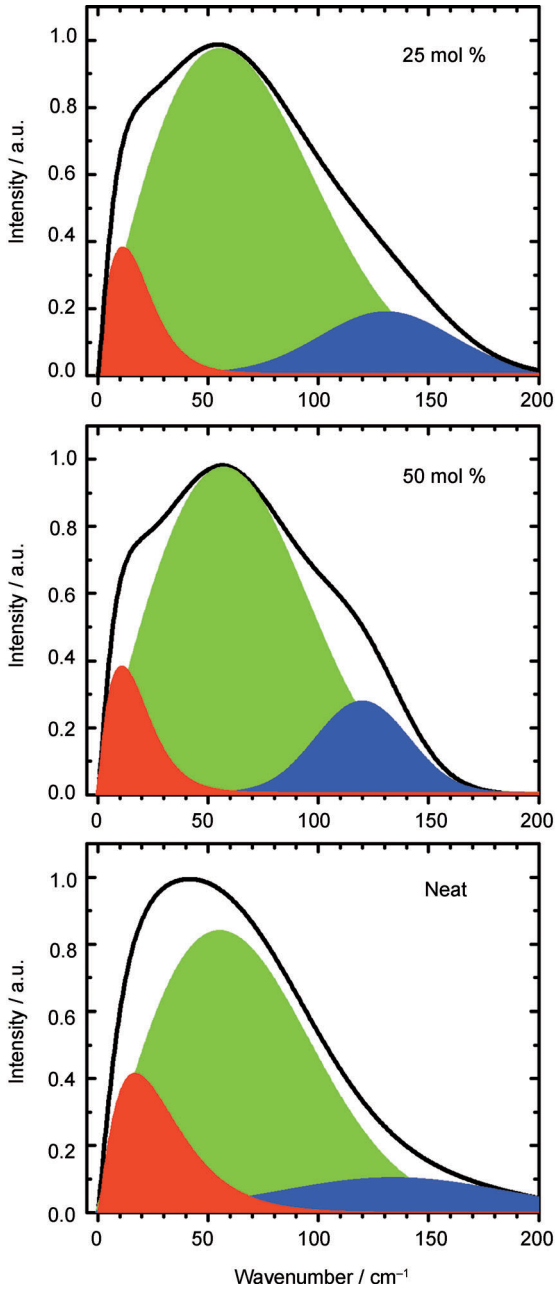

Figure 15. Comparison of the intermolecular spectra of CH_3CN in 25 and 50 mol% $CH_3CN/[C_5mim][NTf_2]$ and in neat CH_3CN with component bands obtained from multicomponent line-shape analysis. See Table 4 for fit parameters.

CH_3CN–cation interactions at this composition. However, with three molecules of CH_3CN for every ion pair, the presence of CH_3CN molecules most likely affects the ionic networks to the extent that the use Equation (7) in describing the RSDs becomes questionable. Indeed, previous THz spectroscopic studies of CH_3CN/IL mixtures indicate that CH_3CN-rich mixtures behave more like electrolyte solutions than mixtures of two liquids.[37] That the deviation of $I_{mix}^{exp}(\omega)$ from $I_{mix}^{ideal}(\omega)$ on the high-frequency side of the RSD is smaller for the 90 mol% mixture than for the 50 and 75 mol% mixtures would seem to suggest that the mixture is at a critical concentration where CH_3CN–cation interaction effects are being balanced by effects caused by solute-induced disruption of the ionic network.

6. Concluding Remarks

Recently, Fruchey and Fayer[89] used the rotational diffusion of charged and uncharged fluorescent probes to show how dynamics are different in nonpolar domains than in the polar domains. In contrast to the work of Fruchey and Fayer, the results in the current paper, as well as that of our previous papers on $CS_2/[C_5mim][NTf_2]$ mixtures, provide insights into the interactions of small solute molecules with ILs. Solute-solvent interactions are often determined by specific interactions of the solvent with functional groups on the solute. Therefore, in order to understand, for example, the effect of ILs on reactions, it is important to understand the interactions of small solute molecules that mimic the functional groups on larger molecules.

Herein, the nanostructural organization and subpicosecond intermolecular dynamics of $CH_3CN/[C_5mim][NTf_2]$ mixtures as a function of composition were investigated by MD simulations and by OHD-RIKES. The simulations show that CH_3CN molecules tend to be located in the interfacial regions between the ionic networks and the nonpolar domains, in accordance with previous MD simulations.[34,76] Moreover, the CH_3CN molecules are oriented with the negatively charged nitrogen atom pointing toward the positively charged headgroup of the cation. We see no evidence for aggregation of the CH_3CN molecules with increasing concentration, which is consistent with the complete miscibility of CH_3CN with ILs.[72,73]

The RSDs of the mixtures narrow and shift to lower frequency with increasing concentration of CH_3CN. Within the context of an additivity model [Eq. (6)], this behavior is mainly attributed to the increase in the contribution of the narrower and lower frequency CH_3CN component to the RSDs of the mixtures. We attribute deviations from additivity to the competition between solute-cation interactions and solute-induced disruption of the ionic networks. Using a modification of the additivity model [Eq. (7)], we showed that these deviations could be quantitatively accounted for by the intermolecular spectrum of CH_3CN in the mixture being broader and higher in frequency than the intermolecular spectrum of CH_3CN in the neat liquid.

Future research in our laboratories will focus on determining the generality of the additivity model [Eq. (6)] as a framework for explaining the concentration dependence of the RSDs of other aprotic polar solvent/IL systems and the extent to which deviations from the additivity model can be rationalized by the interplay between solute-cation interactions and solute-induced disruption of the ionic network.

Acknowledgements

This research was supported by grants from the National Science Foundation (CHE-0718678) and the American Chemical Society Petroleum Research Fund (47615-AC6) to E.L.Q., The Welch Foun-

dation (D-0775) to R.A.B., and the Air Force Office of Scientific Research to G.A.V.. We thank Lianjie Xue for help with the OKE measurements and Peter Chang for help with the density measurements.

Keywords: ionic liquids · mixtures · molecular dynamics simulations · nanostructural organization · optical Kerr effect

[1] *Ionic Liquids in Synthesis* (Eds.: P. Wasserscheid, T. Welton), Wiley-VCH, Weinheim, **2007**.
[2] N. V. Plechkova, K. R. Seddon, *Chem. Soc. Rev.* **2008**, *37*, 123 – 150.
[3] M. J. Earle, J. M. S. S. Esperanca, M. A. Gilea, J. N. A. C. Lopes, L. P. N. Rebelo, J. W. Magee, K. R. Seddon, J. A. Widegren, *Nature* **2006**, *439*, 831 – 834.
[4] M. Freemantle, *Chem. Eng. News* **1998**, *76*, 32 – 37.
[5] N. V. Plechkova, K. R. Seddon in *Methods and Reagents for Green Chemistry: An Introduction* (Eds.: P. Tundo, A. Perosa, F. Zecchini), Wiley, New York, **2007**, pp. 105 – 130.
[6] Y. Wang, G. A. Voth, *J. Am. Chem. Soc.* **2005**, *127*, 12192 – 12193.
[7] Y. Wang, G. A. Voth, *J. Phys. Chem. B* **2006**, *110*, 18601 – 18608.
[8] J. N. A. Canongia Lopes, A. A. H. Pádua, *J. Phys. Chem. B* **2006**, *110*, 3330 – 3335.
[9] Y. Wang, W. Jiang, G. A. Voth in *Ionic Liquids IV. Not Just Solvents Anymore, Vol. 975* (Eds: J. F. Brennecke, J. D. Rogers, K. R. Seddon), ACS Symposium Series, American Chemical Society, Washington DC, **2007**, pp. 272 – 307.
[10] S. Shigeto, H.-o. Hamaguchi, *Chem. Phys. Lett.* **2006**, *427*, 329 – 332.
[11] K. Iwata, H. Okajima, S. Saha, H.-O. Hamaguchi, *Acc. Chem. Res.* **2007**, *40*, 1174 – 1181.
[12] D. A. Turton, J. Hunger, A. Stoppa, G. Hefter, A. Thoman, M. Walther, R. Buchner, K. Wynne, *J. Am. Chem. Soc.* **2009**, *131*, 11140 – 11146.
[13] A. Triolo, O. Russina, H.-J. Bleif, E. Di Cola, *J. Phys. Chem. B* **2007**, *111*, 4641 – 4644.
[14] A. Triolo, O. Russina, B. Fazio, R. Triolo, E. Di Cola, *Chem. Phys. Lett.* **2008**, *457*, 362 – 365.
[15] C. Hardacre, J. D. Holbrey, C. L. Mullan, T. G. A. Youngs, D. T. Bowron, *J. Chem. Phys.* **2010**, *133*, 074510.
[16] B. Aoun, A. Goldbach, M. A. Gonzalez, S. Kohara, D. L. Price, M.-L. Saboungi, *J. Chem. Phys.* **2011**, *134*, 104509.
[17] D. Xiao, L. G. Hines, Jr., S. Li, R. A. Bartsch, E. L. Quitevis, O. Russina, A. Triolo, *J. Phys. Chem. B* **2009**, *113*, 6426 – 6433.
[18] O. Russina, M. Beiner, C. Pappas, M. Russina, V. Arrighi, T. Unruh, C. L. Mullan, C. Hardacre, A. Triolo, *J. Phys. Chem. B* **2009**, *113*, 8469 – 8474.
[19] O. Russina, A. Triolo, *Faraday Discuss.* **2012**, *154*, 97 – 109.
[20] W. Zheng, A. Mohammed, L. G. Hines, Jr., D. Xiao, O. J. Martinez, S. Simon, R. A. Bartsch, O. Russina, A. Triolo, E. L. Quitevis, *J. Phys. Chem. B* **2011**, *115*, 6572 – 6584.
[21] O. Russina, A. Triolo, L. Gontrani, R. Caminiti, *J. Phys. Chem. Lett.* **2012**, *3*, 27 – 33.
[22] A. Triolo, O. Russina, B. Fazio, G. A. Appetecchi, M. Carewska, S. Passerini, *J. Chem. Phys.* **2009**, *130*, 164521.
[23] C. S. Santos, N. S. Murthy, G. A. Baker, E. W. Castner, Jr., *J. Chem. Phys.* **2011**, *134*, 121101.
[24] S. Li, J. L. Banuelos, J. Guo, L. Anovitz, G. Rother, R. W. Shaw, P. C. Hillesheim, S. Dai, G. A. Baker, P. T. Cummings, *J. Phys. Chem. Lett.* **2012**, *3*, 125 – 130.
[25] M. Mizuhata, M. Maekawa, S. Deki, *ECS Trans.* **2007**, *3*, 89.
[26] L. Gontrani, O. Russina, F. L. Celso, R. Caminiti, G. Annat, A. Triolo, *J. Phys. Chem. B* **2009**, *113*, 9235 – 9240.
[27] C. S. Santos, H. V. R. Annapureddy, N. S. Murthy, H. K. Kashyap, E. W. Castner, Jr., C. J. Margulis, *J. Chem. Phys.* **2011**, *134*, 064501.
[28] R. Atkin, G. G. Warr, *J. Phys. Chem. B* **2008**, *112*, 4164 – 4166.
[29] T. L. Greaves, D. F. Kennedy, S. F. Mudie, C. J. Drummond, *J. Phys. Chem. B* **2010**, *114*, 10022 – 10031.
[30] T. L. Greaves, D. F. Kennedy, N. Kirby, C. J. Drummond, *Phys. Chem. Chem. Phys.* **2011**, *13*, 13501 – 13509.
[31] H. V. R. Annapureddy, H. K. Kashyap, P. M. De Biase, C. J. Margulis, *J. Phys. Chem. B* **2010**, *114*, 16838 – 16846.
[32] H. K. Kashyap, C. S. Santos, H. V. R. Annapureddy, D. S. N. Murthy, C. J. Margulis, E. W. Castner, Jr., *Faraday Discuss.* **2012**, *154*, 133 – 143.
[33] R. Hayes, S. Imberti, G. G. Warr, R. Atkin, *Phys. Chem. Chem. Phys.* **2011**, *13*, 3237 – 3247.
[34] A. A. H. Pádua, M. F. C. Gomes, J. N. A. Canongia Lopes, *Acc. Chem. Res.* **2007**, *40*, 1087 – 1096.
[35] W. Jiang, Y. Wang, G. A. Voth, *J. Phys. Chem. B* **2007**, *111*, 4812 – 4818.
[36] X. Wu, Z. Liu, S. Huang, W. Wang, *Phys. Chem. Chem. Phys.* **2005**, *7*, 2771 – 2779.
[37] M. L. Asaki, A. Redondo, T. A. Zawodzinski, A. J. Taylor, *J. Chem. Phys.* **2002**, *116*, 10377 – 10385.
[38] F. Aliotta, R. C. Ponterio, F. Saija, G. Salvato, A. Triolo, *J. Phys. Chem. B* **2007**, *111*, 10202 – 10207.
[39] D. Chakrabarty, A. Chakrabarty, D. Seth, M. Sarkar, *J. Phys. Chem. A* **2005**, *109*, 1764 – 1769.
[40] D. McMorrow, W. T. Lotshaw, G. A. Kenney-Wallace, *IEEE J. Quantum Electron.* **1988**, *24*, 443 – 454.
[41] E. W. Castner, Jr., M. Maroncelli, *J. Mol. Liq.* **1998**, *77*, 1 – 36.
[42] J. T. Fourkas in *Ultrafast Infrared and Raman Spectroscopy* (Ed.: M. D. Fayer) Marcel Dekker, Inc., New York, **2001**, pp. 473 – 512.
[43] N. Smith, S. R. Meech, *Int. Rev. Phys. Chem.* **2002**, *21*, 75 – 100.
[44] D. McMorrow, *Opt. Commun.* **1991**, *86*, 236 – 244.
[45] D. McMorrow, W. T. Lotshaw, *J. Phys. Chem.* **1991**, *95*, 10395 – 10406.
[46] N. T. Hunt, A. A. Jaye, S. R. Meech, *Phys. Chem. Chem. Phys.* **2007**, *9*, 2167 – 2180.
[47] B. R. Hyun, S. V. Dzyuba, R. A. Bartsch, E. L. Quitevis, *J. Phys. Chem. A* **2002**, *106*, 7579 – 7585.
[48] G. Giraud, C. M. Gordon, I. R. Dunkin, K. Wynne, *J. Chem. Phys.* **2003**, *119*, 464 – 477.
[49] J. R. Rajian, S. Li, R. A. Bartsch, E. L. Quitevis, *Chem. Phys. Lett.* **2004**, *393*, 372 – 377.
[50] H. Shirota, A. M. Funston, J. F. Wishart, E. W. Castner, Jr., *J. Chem. Phys.* **2005**, *122*, 184512.
[51] H. Shirota, E. W. Castner, Jr., *J. Phys. Chem. A* **2005**, *109*, 9388 – 9392.
[52] H. Shirota, E. W. Castner, Jr., *J. Phys. Chem. B* **2005**, *109*, 21576 – 21585.
[53] D. Xiao, J. R. Rajian, S. Li, R. A. Bartsch, E. L. Quitevis, *J. Phys. Chem. B* **2006**, *110*, 16174 – 16178.
[54] D. Xiao, J. R. Rajian, A. Cady, S. Li, R. A. Bartsch, E. L. Quitevis, *J. Phys. Chem. B* **2007**, *111*, 4669 – 4677.
[55] H. Shirota, J. F. Wishart, E. W. Castner, Jr., *J. Phys. Chem. B* **2007**, *111*, 4819 – 4829.
[56] E. W. Castner, Jr., J. F. Wishart, H. Shirota, *Acc. Chem. Res.* **2007**, *40*, 1217 – 1227.
[57] D. Xiao, J. R. Rajian, L. G. Hines, Jr., S. Li, R. A. Bartsch, E. L. Quitevis, *J. Phys. Chem. B* **2008**, *112*, 13316 – 13325.
[58] H. Shirota, K. Nishikawa, T. Ishida, *J. Phys. Chem. B* **2009**, *113*, 9831 – 9839.
[59] H. Shirota, H. Fukazawa, T. Fujisawa, J. F. Wishart, *J. Phys. Chem. B* **2010**, *114*, 9400 – 9412.
[60] F. Hiroki, I. Tateki, H. Shirota, *J. Phys. Chem. B* **2011**, *115*, 4621 – 4631.
[61] H. Shirota, I. Tateki, *J. Phys. Chem. B* **2011**, *115*, 10860 – 10870.
[62] E. W. Castner, Jr., C. J. Margulis, M. Maroncelli, J. F. Wishart, *Ann. Rev. Phys. Chem.* **2011**, *62*, 85 – 105.
[63] D. A. Turton, T. Sonnleitner, A. Ortner, M. Walther, G. Hefter, R. Buchner, K. Wynne, *Faraday Discuss.* **2012**, *154*, 145 – 153.
[64] P. Yang, G. A. Voth, D. Xiao, L. Hines, R. A. Bartsch, E. L. Quitevis, *J. Chem. Phys.* **2011**, *135*, 034502.
[65] D. Xiao, L. G. Hines, Jr., R. A. Bartsch, E. L. Quitevis, *J. Phys. Chem. B* **2009**, *113*, 4544 – 4548.
[66] J. N. Canongia Lopes, A. A. H. Padua, *J. Phys. Chem. B* **2004**, *108*, 16893 – 16898.
[67] C. I. Bayly, P. Cieplak, W. Cornell, P. A. Kollman, *J. Phys. Chem.* **1993**, *97*, 10269 – 10280.
[68] Gaussian 03 (Revision C.02), M. J. Frisch, G. W. Trucks, H. B. Schlegel, G. E. Scuseria, M. A. Robb, J. R. Cheeseman, J. Montgomery, J. A., T. Vreven, K. N. Kudin, J. C. Burant, J. M. Millam, S. S. Iyengar, J. Tomasi, V. Barone, B. Mennucci, M. Cossi, G. Scalmani, N. Rega, G. A. Petersson, H. Nakatsuji, M. Hada, M. Ehara, K. Toyota, R. Fukuda, J. Hasegawa, M. Ishida, T. Nakajima, Y. Honda, O. Kitao, H. Nakai, M. Klene, X. Li, J. E. Knox, H. P. Hratchian, J. B. Cross, C. Adamo, J. Jaramillo, R. Gomperts, R. E. Stratmann, O. Yazyev, A. J. Austin, R. Cammi, C. Pomelli, J. W. Och-

terski, P. Y. Ayala, K. Morokuma, G. A. Voth, P. Salvador, J. J. Dannenberg, V. G. Zakrzewski, S. Dapprich, A. D. Daniels, M. C. Strain, O. Farkas, D. K. Malick, A. D. Rabuck, K. Raghavachari, J. B. Foresman, J. V. Ortiz, Q. Cui, A. G. Baboul, S. Clifford, J. Cioslowski, B. B. Stefanov, G. Liu, A. Liashenko, P. Piskorz, I. Komaromi, R. L. Martin, D. J. Fox, T. Keith, M. A. Al-Laham, C. Y. Peng, A. Nanayakkara, M. Challacombe, P. M. W. Gill, B. Johnson, W. Chen, M. W. Wong, C. Gonzalez, J. A. Pople, Gaussian, Inc.: Wallingford, CT, **2004**.

[69] A. M. Nikitin, A. P. Lyubartsev, *J. Comput. Chem.* **2007**, *28*, 2020 – 2026.

[70] W. Smith, T. R. Forester, *The DL_POLY_2_USER MANUAL*, **2008**.

[71] S. V. Dzyuba, R. A. Bartsch, *ChemPhysChem* **2002**, *3*, 161 – 166.

[72] G. Hong, J. Jacquemin, P. Husson, M. F. C. Gomes, M. Deetlefs, M. Nieuwenhuyzen, *Ind. Eng. Chem. Res.* **2006**, *45*, 8180 – 8188.

[73] M. Geppert-Rybczyn'ska, A. Heintz, J. K. Lehmann, A. Golus, *J. Chem. Eng. Data* **2010**, *55*, 4114 – 4120.

[74] T. Fujisawa, K. Nishikawa, H. Shirota, *J. Chem. Phys.* **2009**, *131*, 244519.

[75] G. Giraud, J. Karolin, K. Wynne, *Biophys. J.* **2003**, *85*, 1903 – 1913.

[76] J. N. A. Canongia Lopes, M. F. C. Gomes, A. A. H. Padua, *J. Phys. Chem. B* **2006**, *110*, 16816 – 16818.

[77] J. J. Wang, Y. Tian, Y. Zhao, K. Zhuo, *Green Chem.* **2003**, *5*, 618 – 622.

[78] M. D. Elola, B. M. Ladanyi, A. Scodinu, B. J. Loughnane, J. T. Fourkas, *J. Phys. Chem. B* **2005**, *109*, 24085 – 24099.

[79] D. McMorrow, N. Thantu, J. S. Melinger, S. K. Kim, W. T. Lotshaw, *J. Phys. Chem.* **1996**, *100*, 10389 – 10399.

[80] T. Steffen, N. A. C. M. Meinders, K. Duppen, *J. Phys. Chem. A* **1998**, *102*, 4213 – 4221.

[81] W. T. Lotshaw, D. McMorrow, N. Thantu, J. S. Melinger, R. Kitchenham, *J. Raman Spectrosc.* **1995**, *26*, 571 – 583.

[82] H. Cang, V. N. Novikov, M. D. Fayer, *J. Chem. Phys.* **2003**, *118*, 2800 – 2807.

[83] J. Li, I. Wang, K. Fruchey, M. D. Fayer, *J. Phys. Chem. A* **2006**, *110*, 10384 – 10391.

[84] H. Cang, L. Jie, M. D. Fayer, *J. Chem. Phys.* **2003**, *119*, 13017 – 13023.

[85] O. Russina, A. Triolo, D. Xiao, L. G. Hines, Jr., R. A. Bartsch, E. L. Quitevis, L. Gontrani, R. Caminiti, N. V. Plechkova, K. R. Seddon, *J. Phys. Condens. Matter* **2009**, *21*, 424121.

[86] Note that the intensities of the lines between 260 and 360 cm^{-1}, which primarily correspond to intramolecular vibrations of $[NTf_2]^-$ do not vary systematically with concentration in the same way as the band in the 0–200 cm^{-1} region. We attribute this behavior to experimental error due to the noise being comparable in amplitude to the oscillations in the OHD-RIKES signal arising from these intramolecular vibrations.

[87] C. Kalpouzos, D. McMorrow, W. T. Lotshaw, G. A. Kenney-Wallace, *Chem. Phys. Lett.* **1988**, *150*, 138 – 146.

[88] C. Kalpouzos, D. McMorrow, W. T. Lotshaw, G. A. Kenney-Wallace, *Chem. Phys. Lett.* **1989**, *155*, 240 – 242.

[89] K. Fruchey, M. D. Fayer, *J. Phys. Chem. B* **2010**, *114*, 2840 – 2845.

Received: January 12, 2012
Published online on April 23, 2012

